JOURNAL OF GEOPHYSICAL RESEARCH, VOL. 105, NO. B3, PAGES 6237–6254, MARCH 10, 2000

Depth-dependent structure of the Landers fault zone from trapped waves generated by aftershocks

Yong-Gang Li[1], John E. Vidale[2], Keiiti Aki[1,3], and Fei Xu[2]

Abstract. We delineate the internal structure of the Johnson Valley and Kickapoo faults (Landers southern rupture) at seismogenic depth using fault zone trapped waves generated by aftershocks. Trapped waves recorded at the dense linear seismic arrays deployed across and along the surface breaks of the 1992 *M*7.5 Landers earthquake show large amplitudes and dispersive wave trains following the *S* waves. Group velocities of trapped waves measured from multiple band-pass-filtered seismograms for aftershocks occurring at different depths between 1.8 km and 8.2 km show an increase in velocity with depth. Velocities range from 1.9 km/s at 4 Hz to 2.6 km/s at 1 Hz for shallow events, while for deep events, velocities range from 2.3 km/s at 4 Hz to 3.1 km/s at 1 Hz. Coda-normalized amplitude spectra of trapped waves peak in amplitudes at 3-4 Hz for stations located close to the fault trace. The amplitude decays rapidly with the station offset from the fault zone. Normalized amplitudes also decrease with distance along the fault, giving an apparent Q of 30 for shallow events and 50 for deep events. We evaluated depth-dependent fault zone structure and its uncertainty from these measurements plus our previous results from near-surface explosion-excited trapped waves [*Li et al.*, 1999] in a systematic model parameter-searching procedure using a three-dimensional (3-D) finite difference computer code [*Graves*, 1996]. Our best model of the Landers fault zone is 250 m wide at the surface, tapering to 100-150 m at 8.2 km depth. The shear velocity within the fault zone increases from 1.0 to 2.5 km/s and Q increases from 20 to 60 in this depth range. Fault zone shear velocities are reduced by 35 to 45% from those of the surrounding rock and also vary along the fault zone with an increase of ~10% near ends of the southern rupture zone.

1. Introduction

Major crustal faults are often marked by zones of lowered velocity with a width of a few hundred meters to a few kilometers [*Thurber*, 1983; *Cormier and Spudich*, 1984; *Mooney and Ginzburg*, 1986]. Evidence for internal structure of faults has come from inactive exhumed faults [*Chester et al.*, 1993], surface expression of active faults [e.g., *Sieh et al.*, 1993; *Johnson et al.*, 1994], and seismic profiling and tomography [e.g., *Aki and Lee*, 1976; *Lees and Malin*, 1990; *Michelini and McEvilly*, 1991; *Eberhart-Phillips and Michael*, 1993; *Scott et al.*, 1994; *Thurber et al.*, 1997]. The fine internal structure of fault zones is of great interest because it may hold the key to understanding the initiation, propagation, and termination of rupture [*Aki*, 1979; *Mooney and Ginzburg*, 1986; *Scholz*, 1990; *Kanamori*, 1994]. Observations suggest that fault zone complexity may segment fault zones [*Lindh and Boore*, 1974; *Aki*, 1984; *Malin et al.*, 1989; *Beck and Christensen*, 1991; *Li et al.*, 1994a, b] or control the timing of moment release in earthquakes [*Campillo and Archuleta*, 1992; *Harris and Day*, 1993; *Wald and Heaton*, 1994]. The strength of the low-velocity anomalies might vary over the earthquake cycle [*Vidale et al.*, 1994; *Marone et al.*, 1995; *Massonnet et al.*, 1996; *Li et al.*, 1998a]. Rupture models have been proposed that involve variations in fluid pressure over the earthquake cycle [*Sibson*, 1977; *Blanpied et al.*, 1992]. For all these models, knowledge of spatial and temporal variations in fault structure will help predict the behavior of future earthquakes, and such knowledge will help to evaluate the models as well.

In the past decade, the fine structure of faults has been investigated through fault zone trapped waves generated either by earthquakes or explosions, as long as the sources are located within the fault zone. Since the trapped waves arise from coherent multiple reflections at the boundaries between the low-velocity fault zone and the high-velocity surrounding rock, these waves are able to probe the internal structure and continuity of the fault zone at depth [*Li*, 1988; *Li and Leary*, 1990; *Leary et al.*, 1991a; *Li and Vidale*, 1996; *Ben-Zion*, 1998]. Trapped waves have been used to resolve the fault zone width of tens to several hundreds of meters at active faults [e.g., *Li et al.*, 1990; *Leary et al.*, 1991b; *Li et al.*, 1994a, b; *Hough et al.*, 1994; *Malin and Lou*, 1995; *Jongmans and Malin*, 1995; *Li et al.*, 1997a, b, 1998b]. From the point view of fracture mechanics [e.g., *Rice*, 1980; *Papageorgiou and Aki*, 1983; *Scholz*, 1990] we interpret that the low-velocity, low-Q zone inferred from trapped wave data is a result of the dynamic rupture in major earthquakes occurred on these active faults.

Thus far, research into fault zone structure using trapped waves has documented the average properties and the continuity of the fault zone. For example, observations and modeling of 3-6 Hz trapped waves from Landers aftershocks revealed a low-velocity waveguide extending along the 30-km-long Landers southern rupture but disconnected from another waveguide on the northern rupture owing to a fault step over between them. The waveguide on the southern rupture, to a depth of 10 km, averages ~180 m in width with an average *S*

[1]Department of Earth Sciences, University of Southern California, Los Angeles.
[2]Department of Earth and Space Sciences, University of California, Los Angeles.
[3]Also at Observatoire du Piton de la Fournaise, La Reunion, France.

Paper number 1999JB900449.
0148-0227/00/1999JB900449$09.00

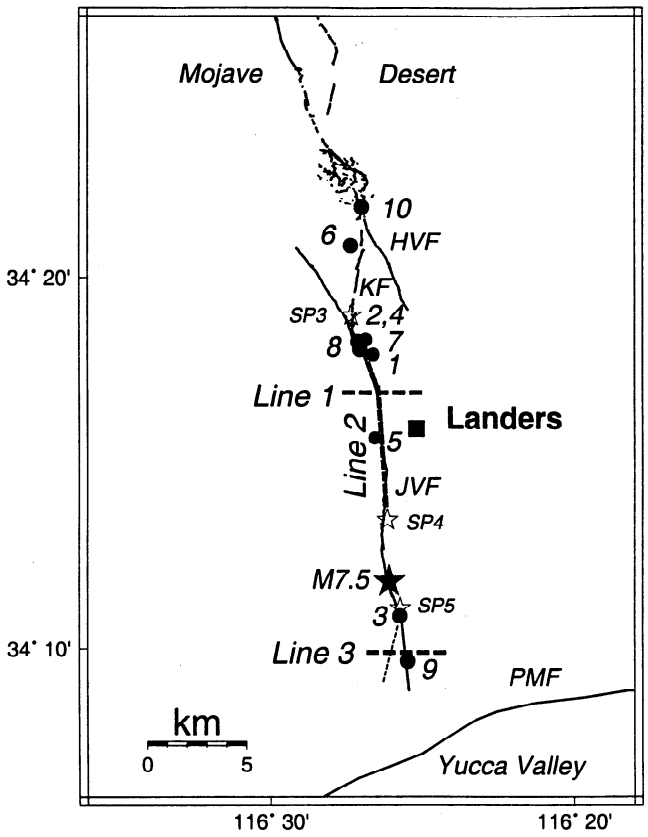

Figure 1. Map of the survey area showing locations of three seismic arrays on lines 1, 2, and 3 (dashed lines) and 10 Landers aftershocks (solid circles), the data from which are used in this study. Line 1 included 35 stations, and line 3 included 21 stations, centered at the main fault trace and with uneven station spacings. Station ST0 at the center of line 1 was located at latitude of 34°16'49.21" and longitude of 116°26'31.84", while station ST0 on line 3 was at 34°09'51.54" and 116°25'29.81". Line 2 included 17 stations with the station spacing of ~500 m along the fault zone. Line 2 intersected line 1 at station ST0. Solid star shows location of the 1992 *M*7.5 Landers, California, earthquake. Open stars show locations of explosions to generate fault zone trapped waves in the previous experiment [*Li et al.*, 1999]. Only the southern half of Landers rupture lies within this map. JVF, Johnson Valley fault; KF, Kickapoo fault, HVF, Homestead Valley fault; PMF, Pinto Mountain fault.

velocity of 2 km/s and Q of 30-50 [*Li et al.*, 1994a, b]. However, we expect that the increasing pressure with increasing depth will strongly affect the crack density, fluid pressure, and amount of fluids, as well as the rate of healing of damage caused by earthquakes. It may also influence the development of fault gouge. Because of all these factors a fault zone is probably not uniform with depth. A primary goal of this paper is to quantify the depth dependence of fault zone properties.

Recently, we used ~2-Hz trapped waves excited by near-surface explosions detonated within the Landers southern rupture zone on the Johnson Valley fault (JVF) and recorded at the dense linear seismic arrays deployed along and across the fault to document the fine structure of the fault to a depth of a few kilometers. Modeling of these trapped waves revealed that the shallow JVF to depth ~1 km is 250 m wide in which the S velocity is 1 km/s and Q is 20, below which the fault zone is narrower and the S velocity increases to ~1.9 km/s and Q to ~30 [*Li et al.*, 1999]. This helps us understand the development of the fault at shallow depths and is also necessary for stripping off shallow effects to resolve internal fault zone structure deeper in the seismogenic zone, as we do in this paper.

In the present study, we used trapped waves generated by aftershocks occurring within the Johnson Valley fault and Kickapoo fault (KF) to find the deeper structure of the Landers southern rupture zone. We present group velocities of trapped waves measured in the frequency range of 1-5 Hz from recorded seismograms for 10 aftershocks occurring at depths between 1 and 8.2 km. We also show fault zone Q values measured from the attenuation of coda normalized spectral amplitudes of trapped waves with distance along the fault. These measurements show an increase in velocity and Q with depth. We next use a three-dimensional (3-D) finite difference code [*Graves*, 1996] to synthesize trapped waves for a model with a realistic geometry of the fault zone and sources. The measured group velocities and Q values are used as constraints in the modeling. In combination with the results from explosion-excited trapped waves, we construct a 3-D model with the depth-variable structure for the Landers fault zone.

2. Data Analysis

Figure 1 shows locations of the three linear seismic arrays deployed across and along the Johnson Valley fault. Lines 1 and 3 were ~3 km in length across the JVF. Line 2 is 8 km in length along the JVF between lines 1 and 3. We used three-channel refraction technology (REFTEK) recorders from the Program for Array Seismic Studies of the Continental Lithosphere (PASSCAL) Instrument Center of Incorporated Research Institutions for Seismology (IRIS). Sensors (Mark Products 2 Hz L22) were buried with the three components aligned vertical, parallel, and perpendicular to the fault trace. These seismic arrays were the same as used to record trapped waves generated by explosions in the Landers rupture zone [*Li et al.*, 1999]. Table 1 gives the times and locations of 10 aftershocks occurring within the Landers fault zone, from which we recorded trapped waves for this study.

Table 1. Times and Locations of Landers Aftershocks in this Data Set

Event	Julian Day	Date	Origin Time UT	Latitude N	Longitude W	Depth km	Magnitude
1	224	Aug. 11, 1996	0435:34.47	34°17.96'	116°26.50'	1(?)	1.2
2	224	Aug. 11, 1996	0546:46.38	34°18.31'	116°26.86'	8.01	1.9
3	225	Aug. 12, 1996	1839:54.48	34°10.88'	116°25.75'	1.75	1.3
4	226	Aug. 12, 1996	0026:23.81	34°18.26'	116°26.64'	8.16	1.3
5	226	Aug. 13, 1996	0640:13.23	34°15.65'	116°26.66'	5.50	1.0
6	226	Aug. 13, 1996	1018:25.07	34°20.83'	116°27.56'	3.20	1.5
7	289	Aug. 16, 1996	0146:46.38	34°18.25'	116°27.02'	6.20	1.9
8	290	Aug. 17, 1996	0451:21.23	34°18.27'	116°27.34'	4.85	1.3
9	291	Aug. 18, 1996	0621:22.75	34°09.72'	116°25.49'	3.50	1.2
10	291	Aug. 18, 1996	0930:14.02	34°21.85'	116°27.00'	6.77	1.0

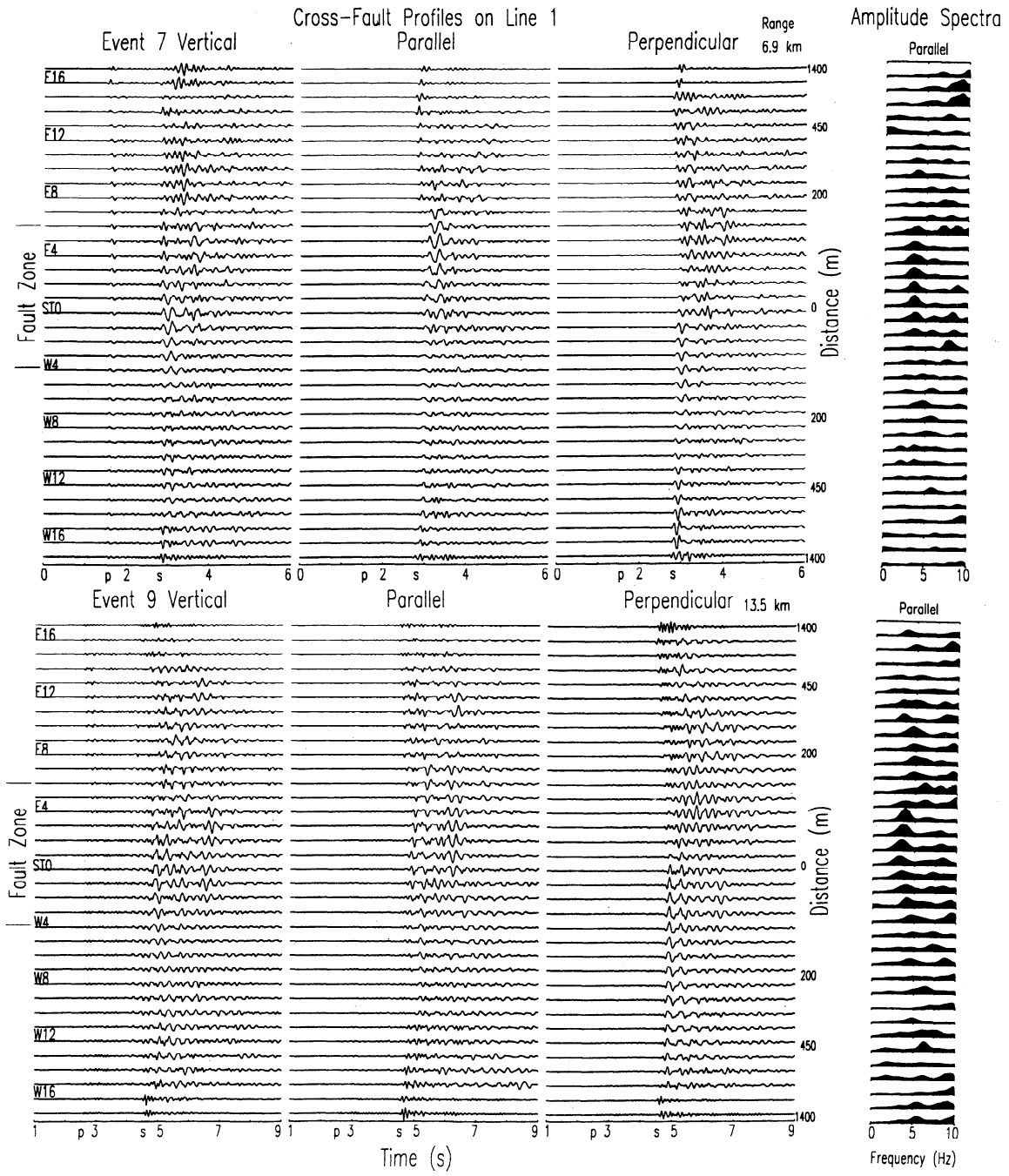

Figure 2. Vertical, fault zone parallel and fault zone perpendicular seismograms recorded on line 1 for two aftershocks occurring within the Landers fault zone. (top) Event 7 located at 6.2 km depth and 3 km north of line 1. bottom: event 9 located at 3.5 km depth and 13 km south of line 1. Range denotes the hypocentral distance between the event and seismic array. Seismograms are plotted using a fixed amplitude scale for all traces in each panel. The ratio of scales for three components is 1:2:1.5. Different timescales are used for two events. *P* and *S* arrivals are denoted. Station spacing of the array was not even, 25 m spacing for the 16 stations located closest to the fault trace but 50 to 250 m spacing for farther stations. Stations with names initiated by E were located at the east side of the fault trace, while those initiated by W were located at the west side of the fault trace. Two solid bars mark the distance range in which fault zone trapped waves are prominent, particularly in fault zone parallel component profiles. Coda-normalized amplitude spectra of trapped waves are plotted using a fixed amplitude scale of 120 for event 7 and 60 for event 9. The peak amplitudes at 3-4 Hz appear at stations close to the fault trace.

Figure 2 illustrates three-component seismograms in the cross-fault profiles on line 1 for two aftershocks (events 7 and 9 in Table 1) that occurred within the fault zone. Event 7 was located at the 6.2 km depth and ~3 km north of line 1, while event 9 was located at 3.5 km depth and ~13 km south of line 1. Fault zone trapped waves with relatively large amplitudes and low frequencies following *S* waves were prominent at stations close to the fault trace. The separation between the *S* and trapped waves for event 9 is larger than that for event 7 owing to the greater hypercentral distance between event 9 and line 1.

In order to study the trapped wave quantitatively, we

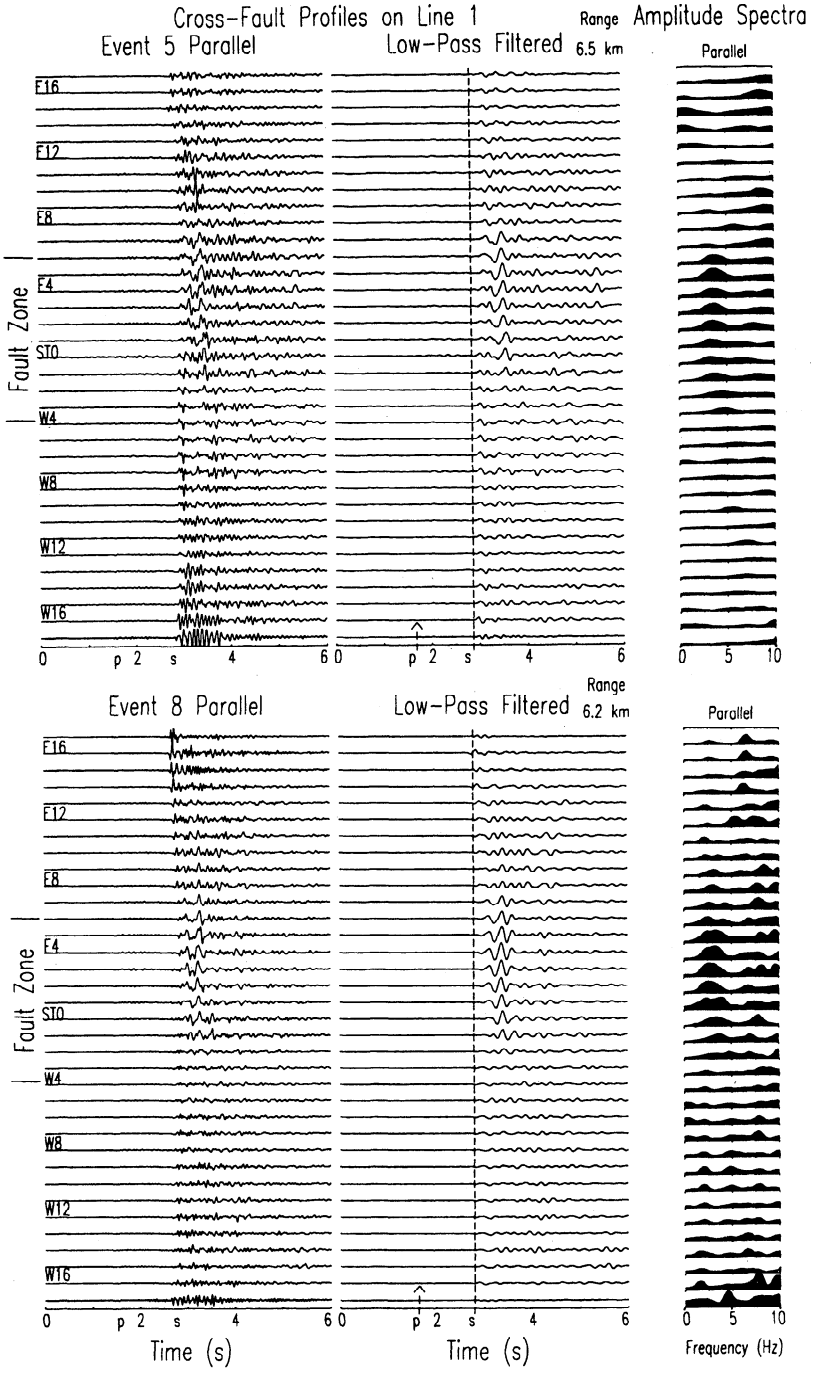

Figure 3a. Fault zone parallel component raw and low-pass- filtered (<6 Hz) seismograms in cross-fault profiles on line 1 for two aftershocks (events 5 and 8) occurring within the Landers fault zone. The two events were located at the similar depths of ~5 km and similar epicentral distances of ~3 km south and north of line 1. Range denotes the hypocentral distance between the event and line 1. The dashed lines in filtered profiles denote *S* arrival times. Trapped waves are prominent at stations close to the fault trace and have the same time delay after *S* waves for these two events. Coda-normalized amplitude spectra of trapped waves are plotted using a fixed amplitude scale of 120 for both events. Other notations are the same as in Figure 2.

calculated the amplitude spectra of trapped waves for a 3-s time window (750 samples for Fourier transformation) starting from the *S* arrivals, using a Hanning window with a 60-ms taper. These spectra were normalized using coda waves to eliminate instrument site and source effects on the spectral amplitudes of trapped waves. The amplitude spectra of coda waves were calculated in a time window with the same length starting at 15 s from the origin time. Normalized amplitude spectra showed a maximum peak at 3-4 Hz at stations close to the fault trace, which decreased rapidly with the station offset from the fault trace (Figure 2). The amplitudes at 3-4 Hz are attributable to trapped waves. On the other hand, stations farther away from the fault zone registered spectral amplitude peak at frequencies >6 Hz owing to less attenuated direct *S* waves. The normalized spectral amplitudes of trapped waves from event 9 are only half as large as those from event 7 because of the more attenuation

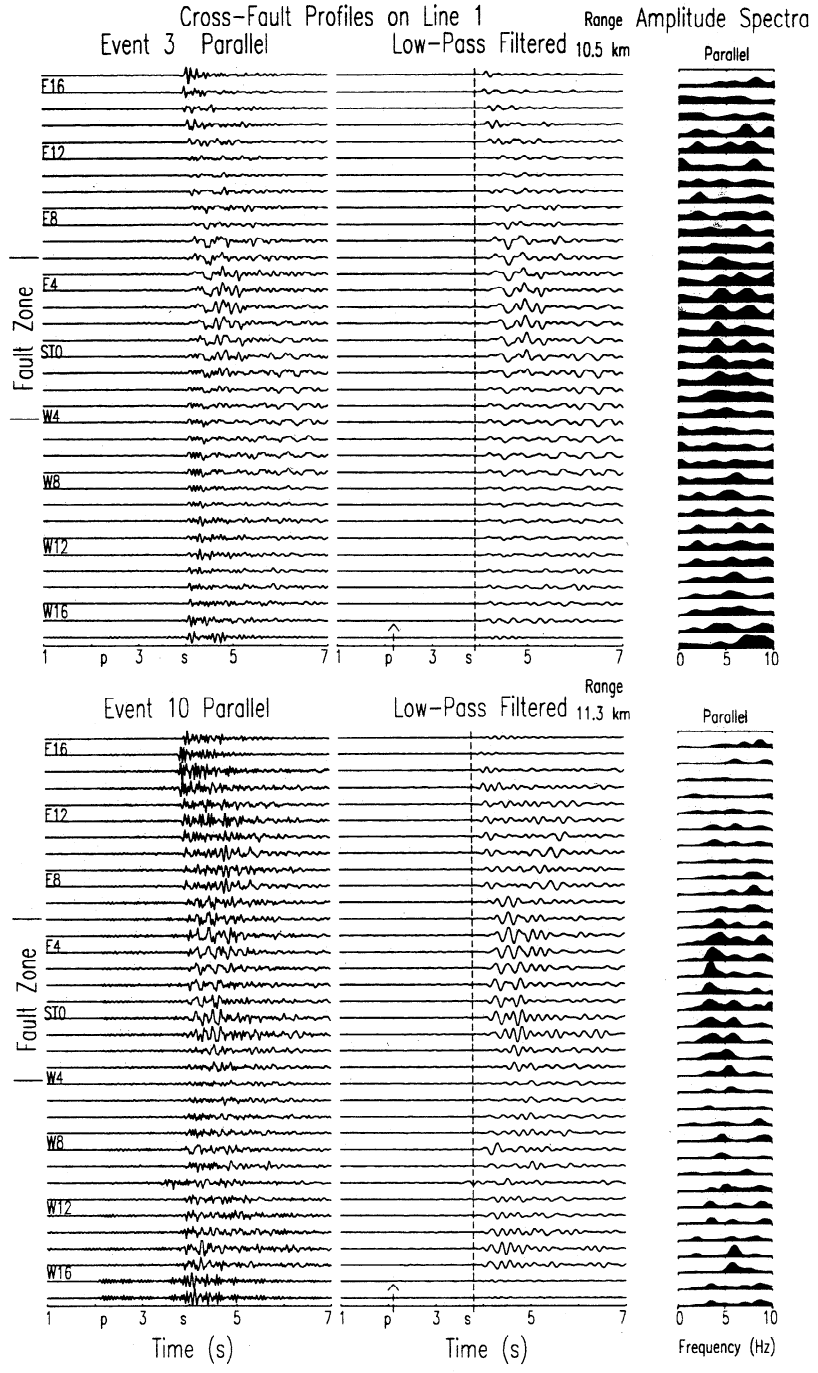

Figure 3b. The data for events 3 and 10 occurring within the Landers fault zone. Event 3 was located at 1.8 km depth and 10 km south of line 1. Event 10 was located at 6.8 km depth and 7 km north of line 1. Trapped waves are prominent at stations close to the fault trace for both events. Separations between *S* and trapped waves for the two events are larger than those for events 5 and 8 because of the longer hypercentral distances. Coda-normalized amplitude spectra of trapped waves are plotted using an amplitude scale of 60 for event 3 and 80 for event 10.

over the longer distance along the fault zone between event 9 and line 1.

Figure 3a illustrates seismograms recorded on line 1 for two aftershocks (events 5 and 8) occurring within the fault zone at the similar depths (5.5 km and 4.9 km) and ~3.5 km south and north of line 1, respectively. Trapped waves are clearly visible at stations close to the fault trace in the low-pass-filtered (<6 Hz) profiles. The separations between *S* and trapped waves for the two events are similar, and the hypercentral distances between the two events and line 1 are almost equal, implying fairly uniform fault-zone waveguide properties in this portion of the fault. Coda-normalized spectral amplitudes show a maximum peak at 3-4 Hz at stations close to the fault trace. The maximum amplitudes for these two events are almost the same.

Figure 3b shows the data recorded on line 1 for two aftershocks (events 3 and 10) occurring within the fault zone. The two events had the similar hypocentral distances to line 1, but event 3 occurred at 1.8 km depth and event 10 occurred at 6.8 km depth. Event 3 was located near the 1992 mainshock

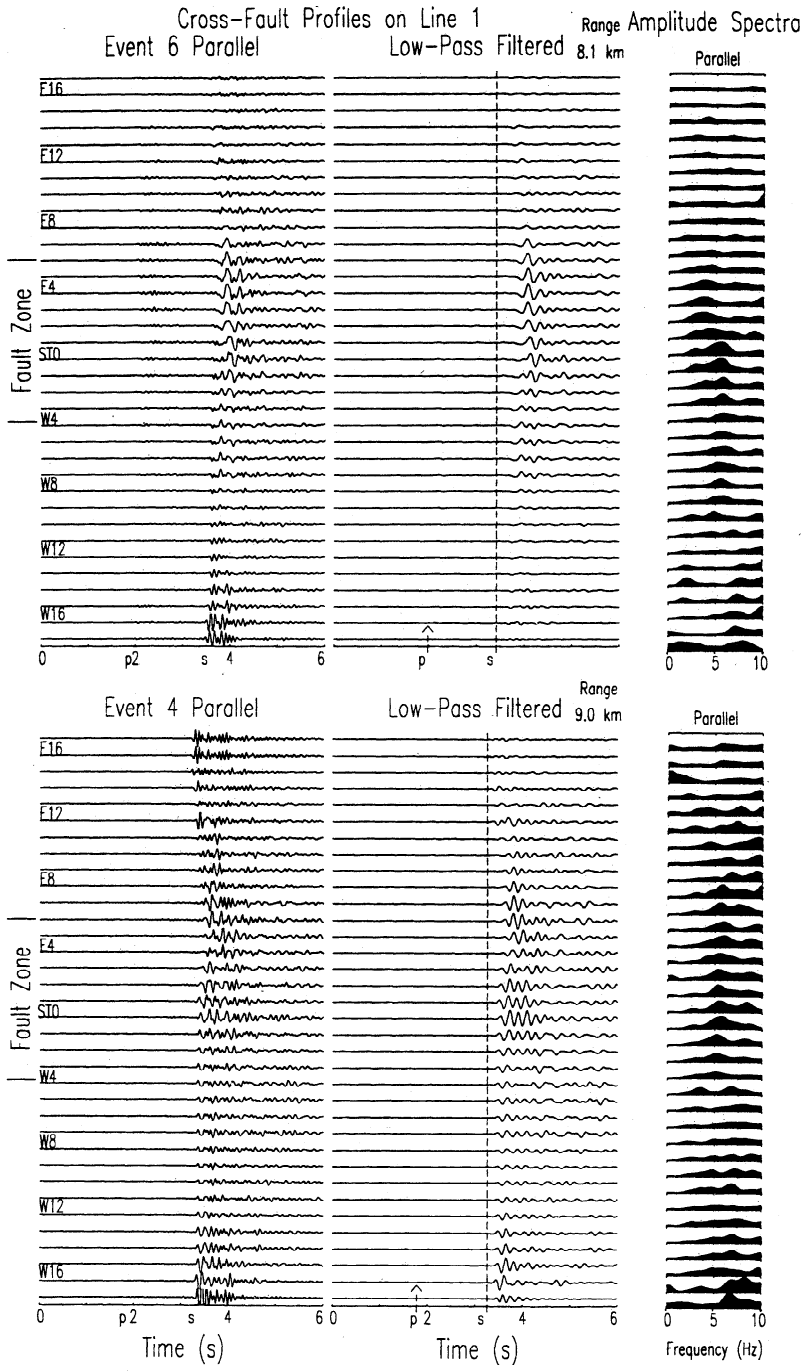

Figure 3c. The data for events 6 and 4. Event 4 was located at 8.2 km depth on the JVF, while event 6 was located at 3.2 km depth on the KF. Trapped waves are prominent at stations close to the fault trace for both aftershocks. Coda-normalized amplitude spectra of trapped waves are plotted using an amplitude scale of 100 for event 4 and 70 for event 6, showing higher frequencies and larger amplitudes for the deeper event 4.

epicenter; in contrast, event 10 was located on the Kickapoo fault near the north end of the Landers southern rupture. We observed prominent trapped waves at 3-4 Hz at stations located close to the fault trace for both aftershocks. The separations between *S* and trapped waves for these two events are larger than those for events 5 and 8 shown in Figure 3a because of the longer hypercentral distances. Coda-normalized spectral amplitudes of trapped waves from event 3 are smaller than those from event 10 owing to the more attenuation at the shallower depth.

We show more examples of trapped waves in Figure 3c for events 4 and 6 occurring on the JVF and the KF, respectively. Event 4 occurred at 8.2 km depth and 3.5 km north of line 1. It is the deepest aftershock used in this study. Event 6 occurred at 3.2 km depth and 7.3 km north of line 1. Trapped waves are prominent at stations close to the fault trace for both events. Seismic waves from the shallower event 6 travel more slowly than those from the deeper event 4, although the distance between event 6 and line 1 is smaller. However, normalized amplitude spectra of trapped waves from the deeper event 4

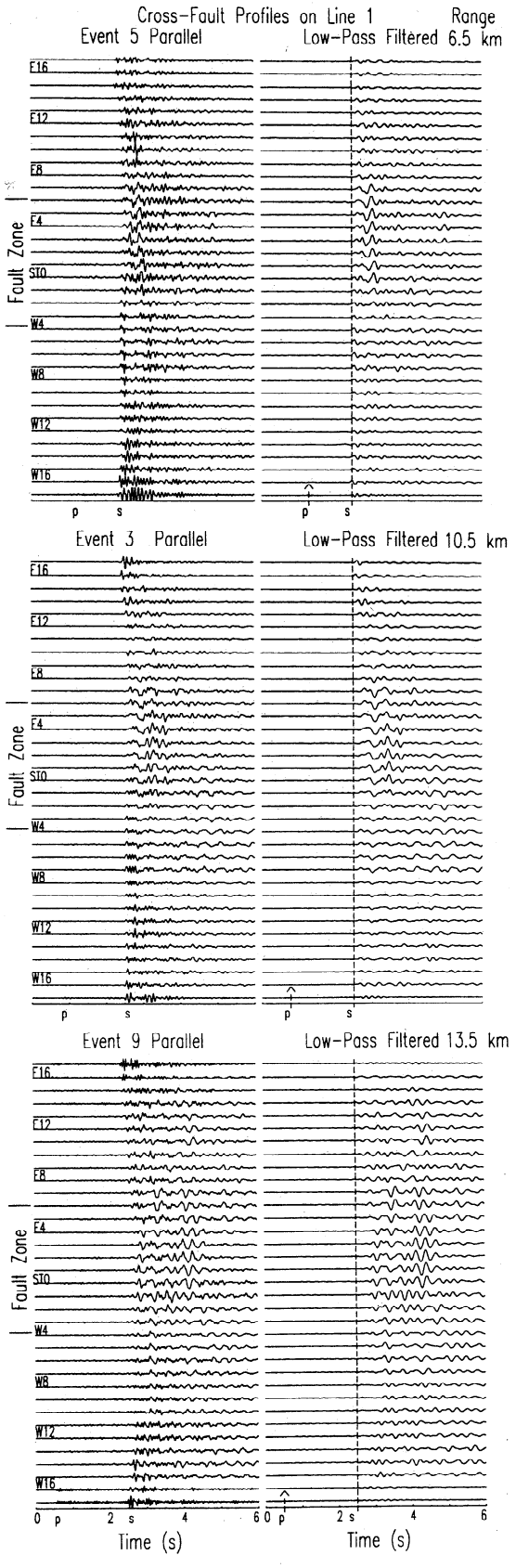

Figure 4. Fault zone parallel component raw and low-pass-filtered (<6 Hz) seismograms on line 1 for events 5, 3, and 9 occurring at depths of 5.5, 1.8, and 3.5 km within the fault zone at hypocentral distances of 6.5, 10.5, and 13.5 km to line 1. The *S* arrivals from three events are aligned (denoted by the dashed lines). The separation between *S* and trapped waves increases with hypercentral distance. Other notations are the same as in Figure 2.

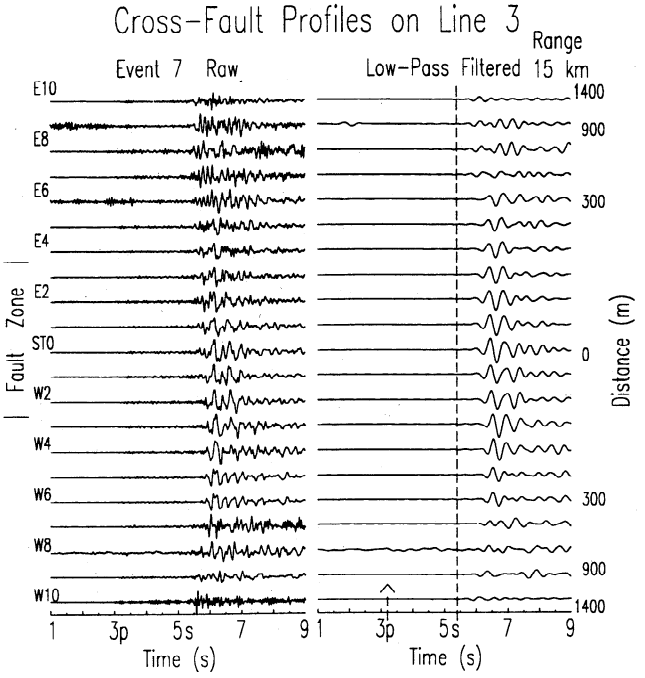

Figure 5. Fault zone parallel component raw and low-pass-filtered (<6 Hz) seismograms on line 3 for event 7 located at 6.2 km depth and 15 km north of line 3. Trapped waves are prominent at stations located within the fault zone. Other notations are the same as in Figure 3.

show a maximum peak at 5-6 Hz, higher than that from event 6. The spectral peak amplitude for event 4 is also larger than that for event 6. These observations imply an increase of fault zone velocity and Q with depth.

Figure 4 shows that the separation between S and trapped waves increases with distance clearly for events 5, 3 and 9, which occurred within the fault zone at distances of 6.5, 10.5, and 13.5 km south of line 1, respectively. The time delay of trapped waves after S-waves increases with the hypocentral distance, as expected for trapped waves traveling along the slower fault zone. Similarly, trapped waves from events 8, 6, and 10 occurring within the fault zone north of line 1 with hypocentral distances of 6.3, 8.0, and 11.3 km (Figure 3) also show an increase in separation between S and trapped waves with distance. Observations of trapped waves from these aftershocks indicate the existence of a continuous low-velocity waveguide at least 25 km long on the Lander southern rupture along the JVF and KF (Figure 1 and Table 1). Focal depths of these aftershocks further suggest that this low-velocity waveguide may extend from the surface to the depth of at least 8.2 km. In our previous study of the Landers fault zone [*Li et al.*, 1994a, b] we found that this waveguide is disconnected from another waveguide on the Landers northern rupture at a fault step over between the Kickapoo fault and the Homestead Valley fault where trapped waves were disrupted, the rupture hesitated [*Wald and Heaton*, 1994], and the slip was minimum [*Sieh et al.*, 1993].

Fault zone trapped waves were also recorded at the seismic array across the southern Johnson Valley fault. For an example, Figure 5 shows seismograms in the cross-fault profiles on line 3 for an aftershock (event 7) occurring within the fault zone at ~15 km north of the array. We observed prominent trapped waves at stations close to the fault zone.

In order to study the dispersion of trapped waves we filtered seismograms using multiple band-pass filters with 0.2 Hz band width. For example, Figure 6 illustrates filtered seismograms recorded on line 1 for three aftershocks (events 6, 3, and 9) in

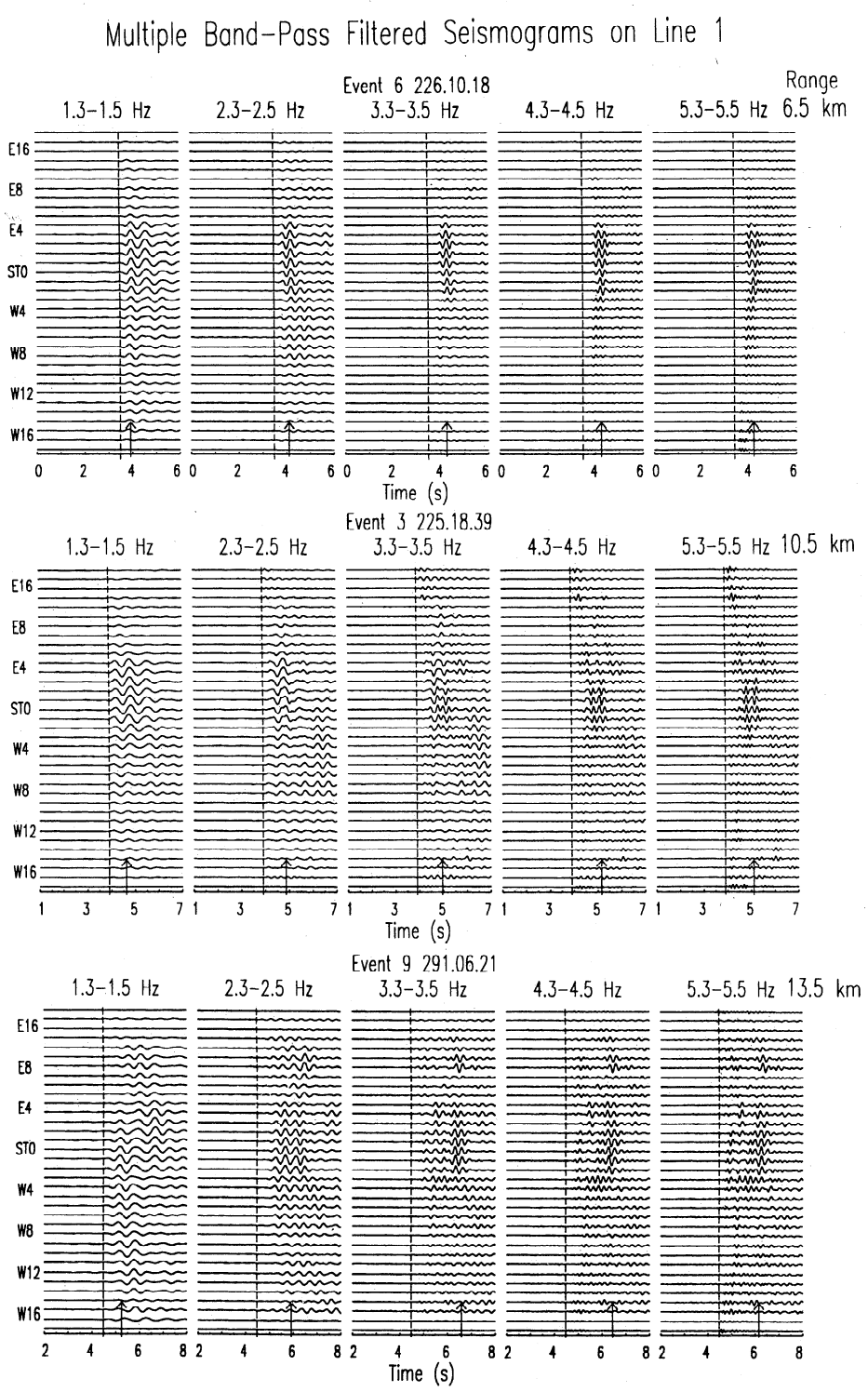

Figure 6. Multiple band-pass-filtered fault zone parallel component seismograms on line 1 for events 6, 3, and 9 in five frequency bands show the dispersion of trapped waves. Events 6, 3, and 9 occurred at depths of 3.2, 1.8, and 3.5 km and at hypocentral distances of 8.1, 10.5, and 13.5 km, respectively. The bandwidth is 0.2 Hz. Filtered seismograms are normalized in each plot. The dashed lines denote the arrivals of *S* waves. Arrows denote the arrivals of trapped waves. Trapped waves at higher frequencies traveled more slowly than those at lower frequencies. Separations between *S* and trapped waves increase with hypercentral distance.

five frequency bands: 1.3-1.5, 2.3-2.5, 3.3-3.5, 4.3-4.5, and 5.3-5.5 Hz. We filtered seismograms using a four-pole Butterworth filter with 0.2-Hz frequency band. Events 6, 3, and 9 occurred within the fault zone at distances of 8.1, 10.5 km, and 13.5 km from line 1, respectively. The separation between *S* and trapped waves increased with the hypercentral distance of events in multiple band-pass-filtered seismograms. Trapped waves at lower frequencies traveled faster than those at higher frequencies, and trapped energy at higher frequencies was more concentrated within the fault zone. Because of this

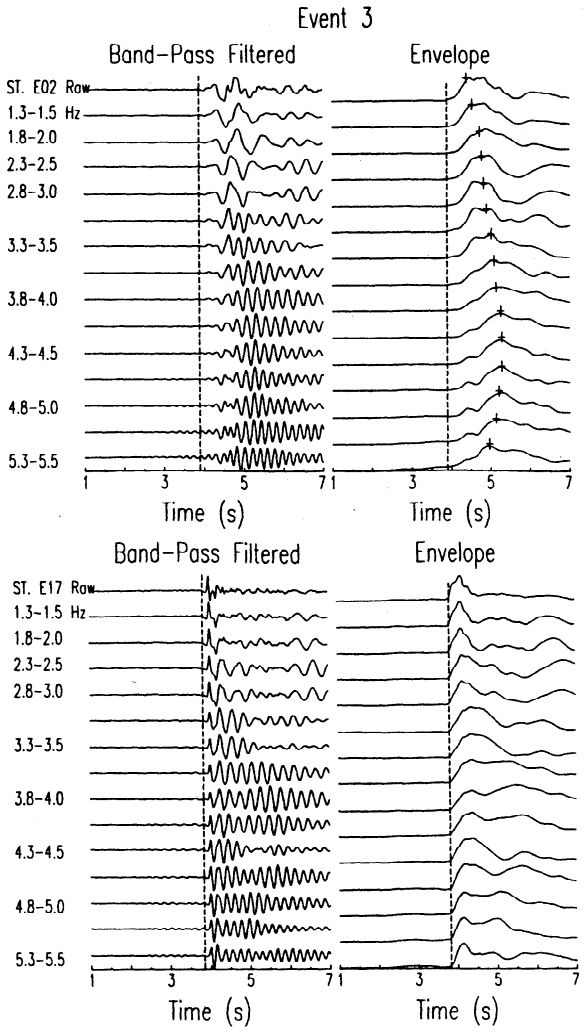

Figure 7a. Multiple band-pass-filtered seismograms from event 3 recorded at two stations. (top) Station E02 located close to the mainshock fault trace. (bottom) Station E17 located 1.2 km away from the fault trace. (left) Fault zone parallel component seismograms filtered in 14 frequency bands are normalized in each plot. (right) Computed envelopes of band-pass-filtered seismograms using a Hilbert transformation. The peak of envelope with a cross indicates the arrival of energy at the specified frequency band. The dispersion is shown in band-pass-filtered seismograms at station E02 but not at station E17. Trapped waves at ~4 Hz traveled most slowly.

dispersion and the concentration of trapped waves within and near the fault zone, these waves can be used as a high-precision probe to delineate the fine structure of the fault zone.

The dispersion of trapped waves is shown more clearly in the following examples. Figure 7a illustrates multiple band-pass-filtered seismograms recorded at station E02 on line 1 for event 3. Seismograms were filtered using a filter with 0.2-Hz band, the center of which moves from 1.4 to 5.4 Hz by a step of 0.5 Hz. Trapped waves are prominent in seismograms because station E02 was located within the fault zone. We calculated the envelope of band-pass-filtered seismograms. The peak in envelope indicates the arrival time of the most energy in the specific frequency band. Filtered seismograms in 14 frequency bands show that trapped waves at higher frequencies traveled more slowly than those at lower frequencies. Trapped waves at ~4 Hz traveled most slowly. In contrast, multiple band-pass seismograms recorded at station

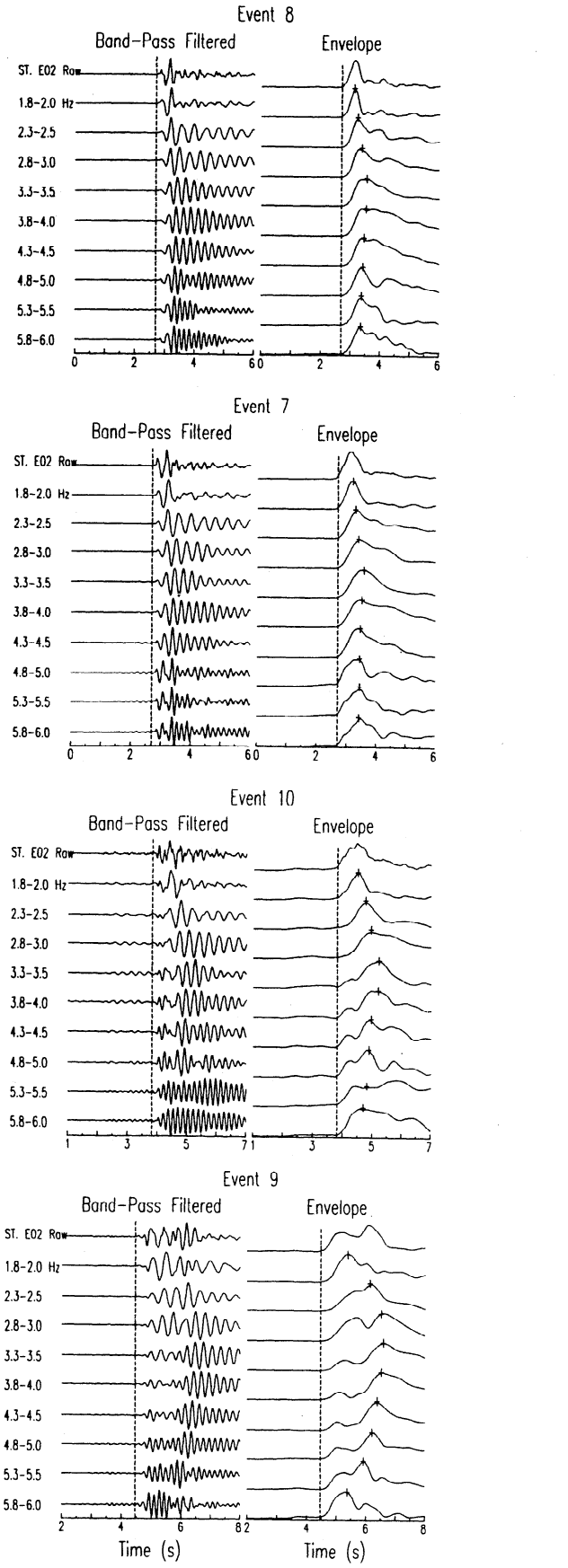

Figure 7b. Multiple band-pass-filtered seismograms recorded at stations within the fault zone for four events 8, 7, 10, and 9 and computed envelopes of band-pass-filtered seismograms showing the dispersion of trapped waves. Trapped waves at 3-4 Hz traveled most slowly. The time delay of trapped waves also increased with hypercentral distance of the event.

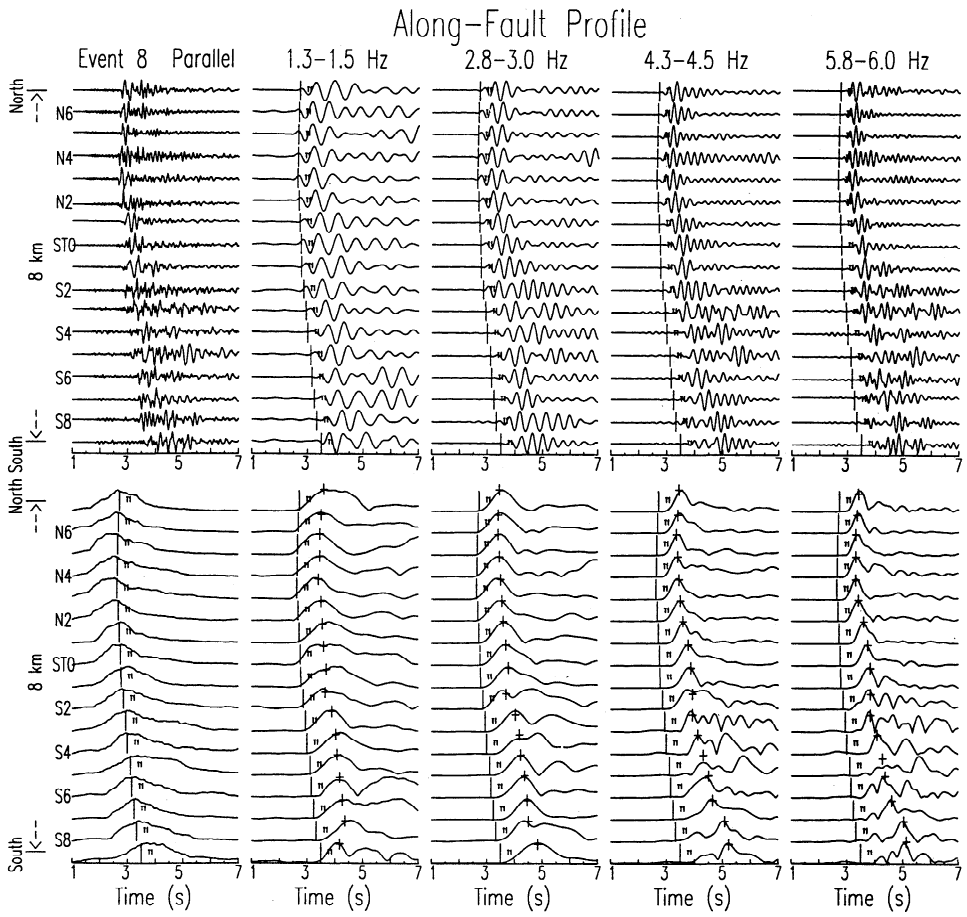

Figure 8. (top) Fault zone parallel component seismograms recorded on line 2 along the Landers fault for an aftershock (event 8) and multiple band-pass-filtered seismograms in four frequency bands show the dispersion of trapped waves. Seismograms are plotted in a trace-normalized profile. The vertical short line labeled by T1 on each trace denotes the *S* arrival. (bottom) Computed envelopes of band-pass-filtered seismograms. The peak of envelope marked by a cross indicates the arrival of trapped energy at the specified frequency band. Trapped waves at higher frequencies traveled more slowly than those at lower frequencies.

E17 located ~1.2 km away from the fault for event 3 show lack of dispersion because this station registered body waves but not trapped waves. Figure 7b illustrates multiple band-pass-filtered seismograms in the frequency range of 1.8 to 6 Hz for four aftershocks (events 8, 7, 10, and 9) with hypercentral distances of 6.2, 6.9, 11.3 km, and 13.5 km to line 1. The dispersion of trapped waves is shown clearly again; trapped waves at higher frequencies traveled more slowly than those at lower frequencies. Events at larger distances to line 1 show the greater delay of trapped waves after *S* waves than those at smaller distances. It is noted that band-pass-filtered seismograms at frequencies higher than 5 Hz are affected by other phases of seismic waves.

Trapped waves recorded on the along-fault line 2 also show the dispersion. For an example, Figure 8 illustrates seismograms recorded at line 2 for an aftershock (event 8) occurring at 4.8 km depth near the north end of line 2. Multiple band-pass-filtered seismograms and the envelopes show that trapped waves at higher frequencies traveled more slowly than those at lower frequencies along the fault zone. The separation between *S* and trapped waves increased with distance between event 8 and stations on line 2.

We then measured group velocities of trapped waves using multiple band-pass-filtered seismograms from seven Landers aftershocks (events 3, 4, 5, 7, 8, 9, and 10 in Table 1) occurring at different depths between 1.8 and 8.2 km within the fault zone. Plate 1 shows group velocities of trapped waves versus frequency for these events. Each point is the mean of measurements in the specified frequency band for the data recorded at five stations on line 1 located close to the fault trace. The data from line 2 were also used when they are available. Line 2 was deployed only for a short time in the experiment so that it did not record all these aftershocks. Group velocities measured for these events range from 1.9 km/s at 4 Hz to 2.6 km/s at 1 Hz for shallow events, while for deep events, velocities range from 2.3 km/s at 4 Hz to 3.1 km/s at 1 Hz, showing dispersion of trapped waves clearly but also implying an increase in fault zone velocity with depth.

In order to evaluate Q values in the fault zone we plotted normalized spectral amplitudes of trapped waves versus hypocentral distances for nine aftershocks in Figure 9. Spectral amplitudes for these events are taken from the computations of coda-normalized amplitude spectra in Figures 2 and 3. Each point in Figure 9 denotes the mean of spectral amplitude peaks between 3 and 5 Hz measured at five stations on line 1 close to the fault. The error bar at each point denotes the standard deviation of measurements. We divided the data into two groups, the first group consisting of events 3, 6, 8, and 9 occurring at depths shallower than 5 km and the second group consisting of events 2, 4, 5, 7, and 10 occurring at

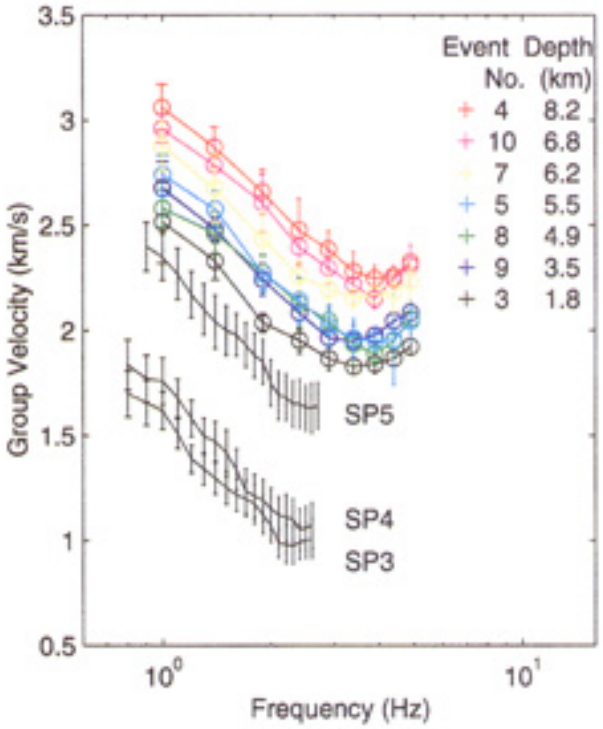

Plate 1. Group velocities of trapped waves measured from multiple band-pass-filtered seismograms for seven aftershocks occurring at different depths between 1.8 and 8.2 km. Each measure point (circle) denotes the mean value of measurements from band-pass-filtered seismograms in the specified frequency band at five stations located within the fault zone. The error bar at each point denotes the standard deviation of measurements; it is smaller than 0.25 km/s. For comparison, group velocities measured from trapped waves excited by explosions SP3, SP4, and SP5 are plotted (adapted from [*Li et al.* 1999]). Measured group velocities of trapped waves imply an increase in velocities with depth.

depths deeper than 5 km. We fit the data using the formula $\ln(A_1/A_i)=\pi f(r_i-r_1)/QV_s$, where A_i is the normalized spectral amplitude for the event located at distance r_i to line 1. The amplitude A_i has been multiplied by a factor $1/\sqrt{r_i}$ to correct geometrical spreading for trapped waves. For shallow events, shear velocity V_s is assumed to be 1.9 km/s and frequency f is 3.8 Hz. For deep events, V_s is assumed to be 2.2 km/s and f is 4.3 Hz. We obtained the best fit to the data using apparent Q of 30 for shallow events while using apparent Q of 50 for deep events, showing that the fault zone Q increases with depth. The measured group velocities and apparent Q values were then used as constraints in our numerical modeling of trapped waves from these aftershocks as described in the following section 3.

3. Three-Dimensional Finite Difference Simulations of Trapped Waves

We used a 3-D finite difference code [*Graves*, 1996] to model fault zone trapped waves with realistic geometry of the fault zone and sources for nine aftershocks in this study. We constructed a 3-D model with the depth-variable structure for the Landers fault zone that matches the combination of measured group velocities and apparent Q values from aftershock-generated trapped waves with the results from explosion-excited trapped waves [*Li et al.*, 1999]. We estimated the uncertainty in the model in a systematic model parameter-searching procedure.

The 3-D finite difference computer code is second order in time and fourth order in space. It propagates the complete wave field through elastic media with a free-surface boundary and spatially variable anelastic damping (an approximate Q). The source can be double couple or an explosion. The first-order elastodynamic equations of motion are solved using a staggered-grid finite difference algorithm. This numerical approach, with a memory optimization procedure, allows large-scale 3-D finite difference problems to be computed on a conventional, single-processor desk-top workstation.

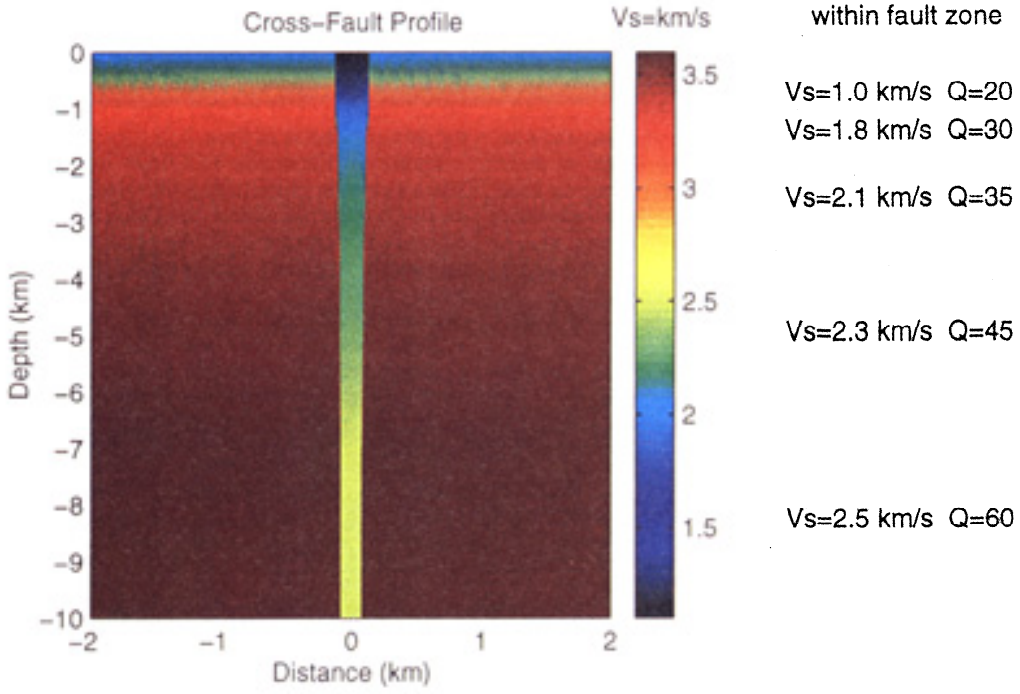

Plate 2. The depth section of structure model across the Landers fault zone. Model parameters were used for the best fit to the data shown in Figures 10 and 11. The fault zone is 250 m wide at the surface and tapered to 125 m at the depth of 10 km. Shear velocities in the fault zone are reduced by 45-35% from those for the surrounding rock from the surface to the 10 km depth. Fault zone velocities and Q increase with depth.

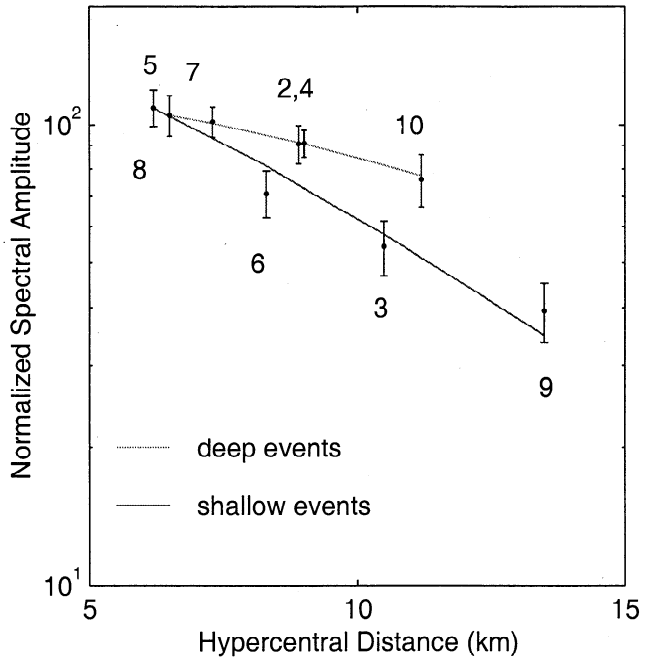

Figure 9. Normalized spectral amplitudes of trapped waves at 3-5 Hz versus hypocentral distances for nine Landers aftershocks. Events are numbered. Each point denotes the mean of coda-normalized spectral amplitude peaks at 3-5 Hz at five stations on line 1 close to the fault trace, which are taken from Figures 2 and 3. We fit the data using the formula $\ln(A_1/A_i)=\pi f(r_i-r_1)/QV_s$. Spectral amplitudes of trapped waves have been multiplied by a factor of $(r_i/r_1)^{1/2}$, i = 1,..., 9, to correct for geometrical spreading. Solid line fits the data for shallow events 3, 6, 8, and 9 using Q of 30, while light line fits the data for deep events 2, 4, 5, 7, and 10 using Q of 50.

The calculation used a 200-by-600-by-500 element grid in x-y-z coordinates, where x and y axes are perpendicular and parallel to the fault trace and z axis is in depth, to simulate a volume of 5 km in width, 15 km in length, and 10 km in depth, which includes the fault zone, all 10 aftershocks, and the seismic array. For the events with shallow depth or short distance from the array we reduced the grid volume to save computation time. The grid spacing is 25 m. The fault zone waveguide is sandwiched between two quarter spaces, and is placed down the middle of the grid, far enough from the edges of the model that side reflections do not appear in the seismograms. The double-couple source can be placed within the fault zone or wall rock.

Because the shallow structure of the Landers fault zone has been delineated using explosion-excited trapped waves [*Li et al.*, 1999], we used it for the top part of the present model. In order to obtain model parameters for the deep part of the fault zone we first fit the data from the shallow aftershock and then fit the data from the deep aftershock. In this way, we obtained the model parameters for layer by layer from the top to the bottom of the model.

To find model parameters that best fit observed trapped waves, we tested various values for the fault zone width, velocity and Q, the wall rock velocity and Q, the layer depths, and the source location in the range shown in Table 2. When the fault zone width varies 25 m (one grid), S velocity varies 0.1 km/s, Q value varies 10, or source offset varies 25 m from the fault, the amplitudes and dispersion of trapped waves change observably. In our previous paper for modeling of trapped waves generated by explosions at the Landers fault zone [*Li et al.*, 1999], we gave the examples to show the sensitivity of these model parameters to synthetic trapped waveforms. The wider fault zone produced trapped waves with lower frequencies. The slower fault zone produced the longer dispersive wave trains of trapped waves. The lower Q fault zone produced trapped waves with smaller amplitudes and shorter wave trains with lower frequencies. However, the variation of wall rock velocities and layer depths mainly affects arrival times of P, S , and trapped waves. The variation of wall rock Q values is less sensitive in modeling.

In the trial-and-error modeling procedure these parameters are not uniquely determined because there is a trade-off among the parameters. For example, an increase of fault zone width is equivalent to the decrease of the fault zone velocity and/or Q value. This problem has been discussed in previous studies for a delineation of fault zone structure using trapped waves [e.g., *Li and Leary*, 1990; *Leary et al.*, 1991b; *Li and Vidale*, 1996; *Ben-Zion*, 1998]. However, the trade-offs can be reduced when we have independent estimates of some parameters. For example, we used the measurements of fault width and velocities in a borehole drilled through the Nojima fault [*Ito*, 1996] as constraints in modeling trapped waves recorded at the Nojima fault from Kobe aftershocks [*Li et al.*, 1998b]. In the present study we used group velocities and Q values measured from the dispersion and attenuation of trapped waves from Landers aftershocks as constraints in the trial-and-error modeling procedure. Table 2 lists the model parameters that best fit the data on the basis of observed dispersive trapped waveforms and S arrival times. Plate 2 displays the depth section of the structure model across the Landers fault zone. Model parameters of the fault zone itself used for the best fit to the data are labeled in Plate 2.

Figure 10 illustrates 3-D finite difference (FD) synthetic seismograms in cross-fault profiles on line 1 for an aftershock (event 7) occurring within the Landers fault zone at depths of 6.2 and 3.5 km north of line 1. Figure 10a shows three-component synthetic seismograms using the best fit model parameters given in Plate 2 and Table 2. Trapped waves with large amplitudes and long-duration wave trains appear only at stations located within and near the fault zone. In this example, trapped waves in fault zone parallel component seismograms show larger amplitudes and are more concentrated within the fault zone than other two components. For a

Table 2. Model Parameters for the Landers Fault Zone

Model Parameters	Best Fit					Tested Range
	Layer 1	Layer 2	Layer 3	Layer 4	Layer 5	
Depth of the layer, km	1.0	1.5	4.0	7.0	10.0	0.5 (step)
Waveguide width, m	250	200	200	150	125	100-250
Waveguide S velocity, km/s	1.0	1.8	2.1	2.3	2.5	1.0-2.5
Waveguide Q value	20	30	35	50	60	20-100
Wall rock velocity, km/s	1.8	3.2	3.4	3.5	3.6	1.8-4.0
Wall rock Q value	35	50	80	120	200	20-200

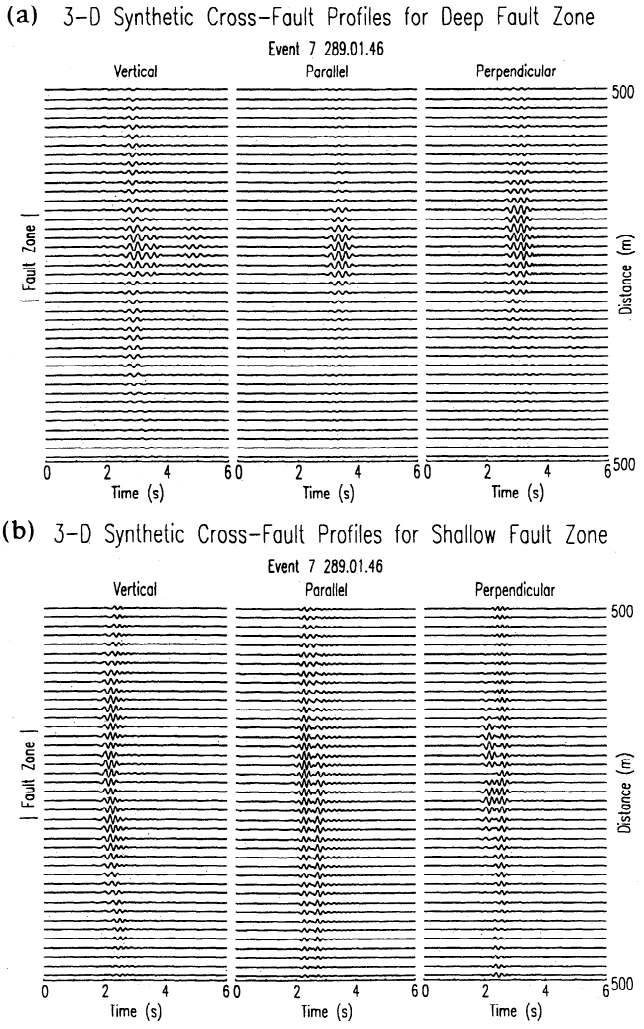

Figure 10. (a) Three components of 3-D finite difference synthetic seismograms in cross-fault profiles on line 1 for an aftershock (event 7) using model parameters for the best fit given in Plate 2 and Table 2. Trace spacing is 25 m. A double-couple source is located at the depth of 6.2 km and 3 km north of the seismic array and 50 m off the middle of the fault zone. The strike and rake angles are 0°, and dip angle is 90°. Synthetic seismograms are plotted using a fixed amplitude scale in each plot. The ratio of scales for three components is 1:5:1. Guided waves with relatively large amplitudes and long-duration waveforms trapped within the fault zone. (b) Three-component synthetic seismograms on line 1 for event 7 using the model with a shallow fault zone only 1 km in the depth. Synthetic seismograms are plotted using a fixed amplitude scale of 5 for all plots. Other parameters are the same as in Figure 10a. In this example, *S* waves are prominent at all stations, but the trapping efficiency of the shallow fault zone structure is weak.

comparison with the result from a shallow fault zone structure, Figure 10b shows synthetic seismograms for event 7 using the same parameters as in the example of Figure 10a but the fault is only 1 km in the depth. In contrast, *S* waves are prominent at all stations of the array, but the trapped waves are not clear because the shallow fault zone has only a weak trapping efficiency. The synthetic seismograms for a shallow fault zone do not match the recorded seismograms.

We have synthesized seismograms for nine Landers aftershocks (Table 1) using a model with depth-variable structure of the fault zone (Plate 2). The model parameters are given in Table 2. Event 2 is not included because events 2 and 4 occurred at almost the same location and showed the similar waveforms. Figure 11 shows fault zone parallel component synthetic seismograms in cross-fault profiles on line 1 for nine aftershocks occurring at different depths and distances from line 1. Synthetic waveforms for all these aftershocks agree well with observed fault zone trapped waves; showing the model in Plate 2 explains our observations of the Landers fault zone. However, we note that in order to obtain the best fit to the data from events 3, 9, and 10 occurring at the south and north ends of the Landers southern rupture zone, respectively, we increased shear velocities of the fault zone by a factor of 10% from those given in Table 2. This infers a variation in velocity along the fault zone.

Finally, we filtered the synthetic seismograms in multiple frequency bands. For example, Figure 12 illustrates synthetic seismograms recorded on line 1 for events 6, 3, and 9 that have been filtered in five frequency bands: 1.3-1.5, 2.3-3.3, 3.3-3.5, 4.3-4.5, and 5.3-5.5 Hz. The band-pass-filtered seismograms show the dispersion of trapped waves clearly. The separation between *S* and trapped waves increases with distance between the events and array. They agree well with the observations (Figure 6), showing that the model parameters given in Plate 2 and Table 2 represent the internal structure of the Landers southern rupture zone.

4. Discussion and Conclusion

In this paper, we have examined the fault zone trapped waves generated by 10 aftershocks occurring at different depths along the Johnson Valley and Kickapoo faults, which ruptured in the *M*7.5 Landers earthquake of 1992. These trapped waves appeared as relatively long-period dispersive wave trains with large amplitudes following *S* waves on seismograms recorded at stations located close to the mainshock fault traces. We measured group velocities of trapped waves from multiple band-pass-filtered seismograms in the frequency range of 1 to 6 Hz for seven Landers aftershocks occurring at depths between 1.8 and 8.2 km. Measured group velocities show dispersion with frequency, and show an increase with depth (Plate 1). These measurements imply an increase in shear velocity of the fault zone with depth.

Coda-normalized amplitude spectra of these trapped waves were a maximum at ~4 Hz, which decayed rapidly with the station offset from the mainshock fault trace and also attenuated along the fault zone. We measured fault zone Q from the amplitude decay of trapped waves at 3-5 Hz with distance along the fault. Results show that the Q value of the fault zone increases with depth too. We obtained apparent Q of 30 by fitting the data for aftershocks occurring at depths shallower than 5 km but Q of 50 for deep aftershocks. The measured Q values may be affected by contamination of other phases, such as *S* waves. However, because *S* waves decay more quickly than trapped waves with distance along the fault zone, the effects of *S* waves on trapped waves are diminished as the distance increases. Using measurements of group velocities and Q values of the fault zone as constraints in modeling allows us to fairly tightly determine the model parameters and to reduce trade-offs among model parameters.

In our previous paper [*Li et al.*, 1999] we used explosion-excited fault zone trapped waves for a delineation of the shallow Johnson Valley fault structure to the depth of ~1 km. The fault is marked by a low-velocity and low-Q zone 250 m wide where the shear velocity is 1 km/s and Q is 20. In the present study we used trapped waves generated by Landers aftershocks for a delineation of the deeper fault zone, including seismogenic depths. Combined with results from explosion-excited trapped waves with the measurements of group velocities and Q values from earthquake-generated trapped

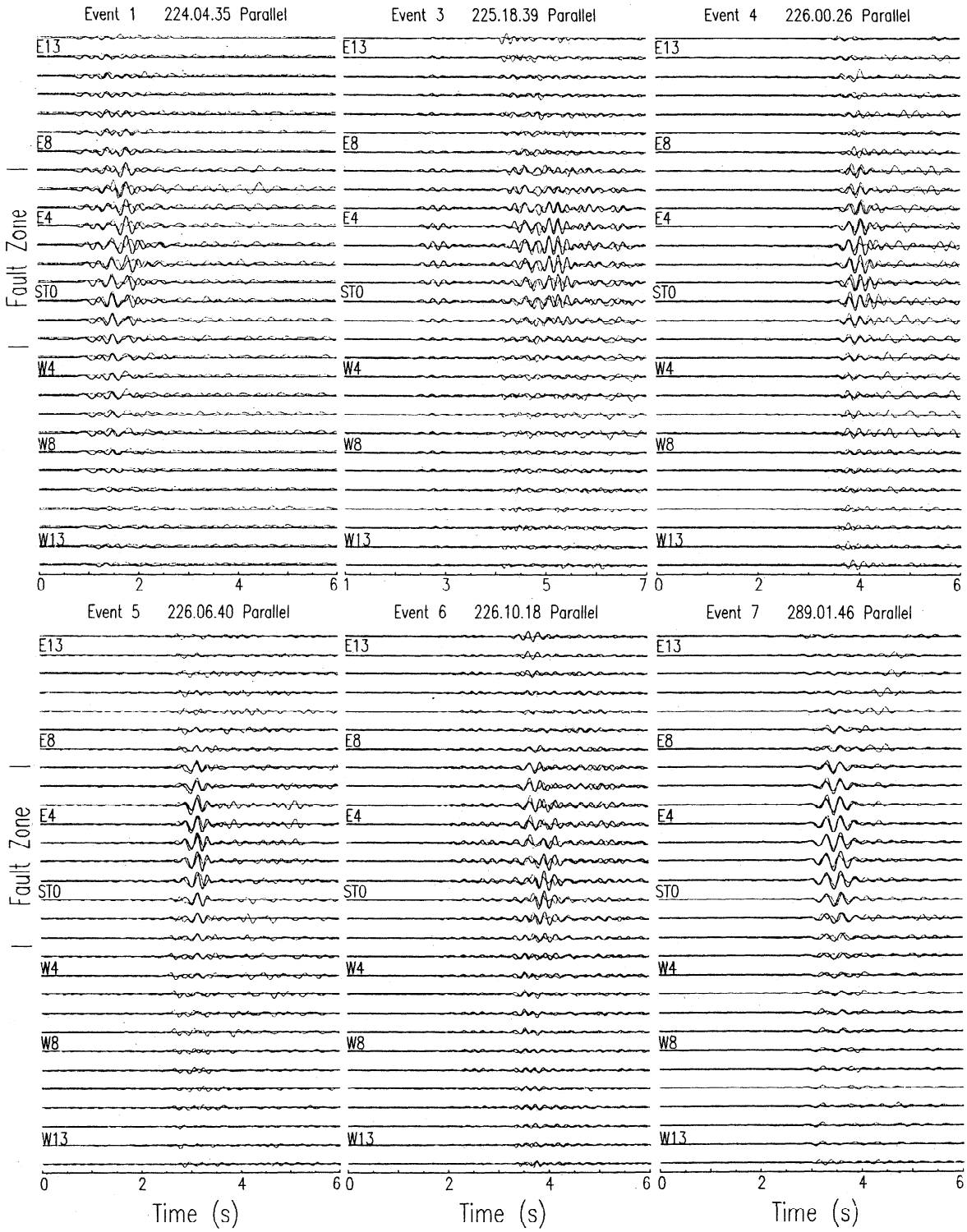

Figure 11. Fault zone parallel component of 3-D finite difference synthetic seismograms (solid lines) on the cross-fault line 1 for nine Landers aftershocks using model parameters that best fit observed trapped waves (light lines). A double-couple source with the strike and rake angles of 0° and dip angle of 90° is located within the fault zone at the hypocentral distance of each event. Both synthetic and recorded seismograms have been low-pass-filtered (<5 Hz) and normalized in each plot. Trace spacings of synthetics are the same as field station spacings.

waves, we constructed a model with depth-variable structure in three-dimensions. We synthesized fault zone trapped waves generated by Landers aftershocks using a 3-D code [*Graves*, 1996] with this model. In a forward model parameter-searching procedure we fit the data from shallow events first and then fit the data from deep events to determine model parameters for layer by layer from the top to bottom of the model. We obtained the best fit to the data using model parameters shown in Plate 2 and Table 2: The fault zone width decreases from 250 to 125 m, shear velocity increases from 1.0 to 2.5 km/s, and Q value increases from 20 to 60 as the depth increases from 0 to ~10 km.

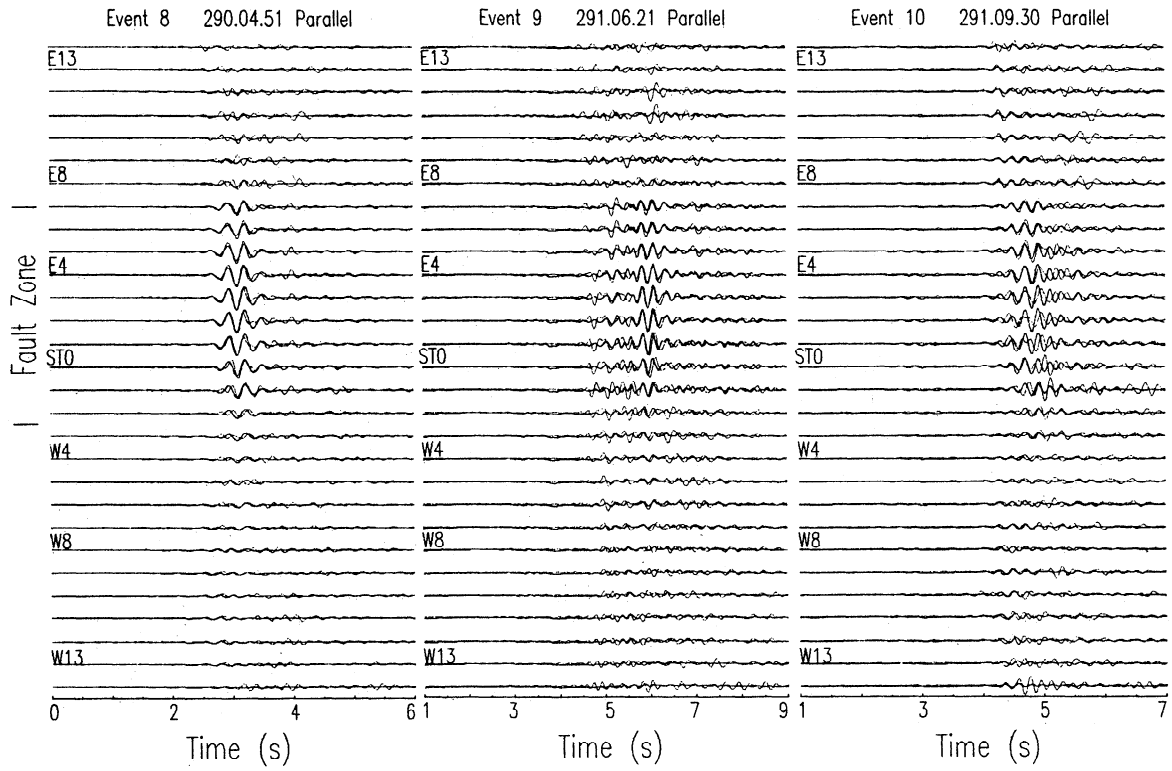

Figure 11. (continued)

A depth-dependent fault zone structure is expected because the increasing pressure with increasing depth will strongly affect the crack density, fluid pressure, and amount of fluids, as well as the rate of healing of damage caused by earthquakes [*Sibson*, 1977, 1982; *Byerlee*, 1990; *Rice*, 1992]. It may also influence the development of fault gouge [*Scholz*, 1990; *Marone*, 1998a, b]. For all these reasons, a realistic fault zone is probably not uniform with depth. It has been shown in this paper that the fault has a narrower width and higher velocities in the deep part than the shallow part. The width of Landers fault zone derived here is consistent with the shear zone spanning all surface breaks around the main trace of the Johnson valley fault as shown in the air photo [*Li et al.*, 1994b, Figure 12] and mapped by *Johnson et al.* [1997]. The width of the fault zone at depth is less constrained in the model parameter searching procedure because the data come from a few deep events in this study.

The numerical modeling of trapped waves for aftershocks occurring at the north end of the Kickapoo fault and the south end of the Johnson Valley fault also revealed that the fault zone shear velocities increase by a factor of ~10% from those shown in Plate 2. Speculatively, the increase in fault zone shear velocity approaching the fault ends infers that the rocks may be more rigid as a result of less accumulated slips near the rupture ends [*Scholz et al.*, 1993]. In our previous study of the Landers fault zone using trapped waves [*Li et al.*, 1994a, b] we have shown that trapped waves were disrupted by the fault step over (barrier) between the Johnson Valley-Kickapoo faults (Landers southern rupture segment) and the Homestead Valley-Emerson Lake faults (the Landers northern rupture segment). The waveguide on the southern rupture is disconnected from the other waveguide on the northern rupture by the fault step over. The fault segmentation along the Landers rupture inferred by trapped waves was also revealed in other research. *Sieh et al.* [1993] and *Johnson et al.* [1994] mapped a minimum in surface slip at this fault step over. *Wald and Heaton* [1994] revealed that the rupture front hesitated as it reached the fault step over in their rupture model for the Landers earthquake. They claim that the rupture hesitation happened within the region of slip transfer from one fault segment to the next. The information on spatial variation in fault zone properties obtained from this study helps us to further understand the fault zone development that we observed at the surface and at seismogenic depths.

From the point view of fracture mechanics the low-velocity waveguide on the ruptured faults may represent the break down zone of inelastic deformation around the propagating crack tip [e.g., *Ida*, 1973; *Rice*, 1980; *Papageorgiou and Aki*, 1983; *Scholz et al.*, 1993; *Marone*, 1998a]. We interpret that the low-velocity waveguide on the Landers fault zone is at least partially caused by the dynamic rupture in the 1992 $M7.5$ earthquake, although it likely also represents a worn zone that has accumulated over geological time [*Cowie and Scholz*, 1992]. *Scholz et al.* [1993], *Schlische et al.* [1996], and *Vermilye and Scholz* [1998] have found the existence of a scale between the dynamic process (cohesive) zone width P and the rupture length L , or the scale between the cataclasite zone width T and the rupture length L. On the basis of our present study we presume the average width of the waveguide to be 200 m on the total 80-km-long Landers rupture length. It gives the ratio of the waveguide width W to the length L to be ~0.004. This ratio is smaller than the predicted scale of 10^{-2} between P and L but larger than the ratio of 10^{-3} between T and L, suggesting that the waveguide width may represent the more intensely fractured cataclasite zone inner the geological process zone wake.

Further, we have observed the increase of ~1-1.5% in fault zone velocities between 2 and 4 years after the mainshock, indicating that the Landers fault is regaining the strength (healing) after the 1992 event [*Li et al.*, 1998a]. This observation supports the existence of earthquake cycle on an

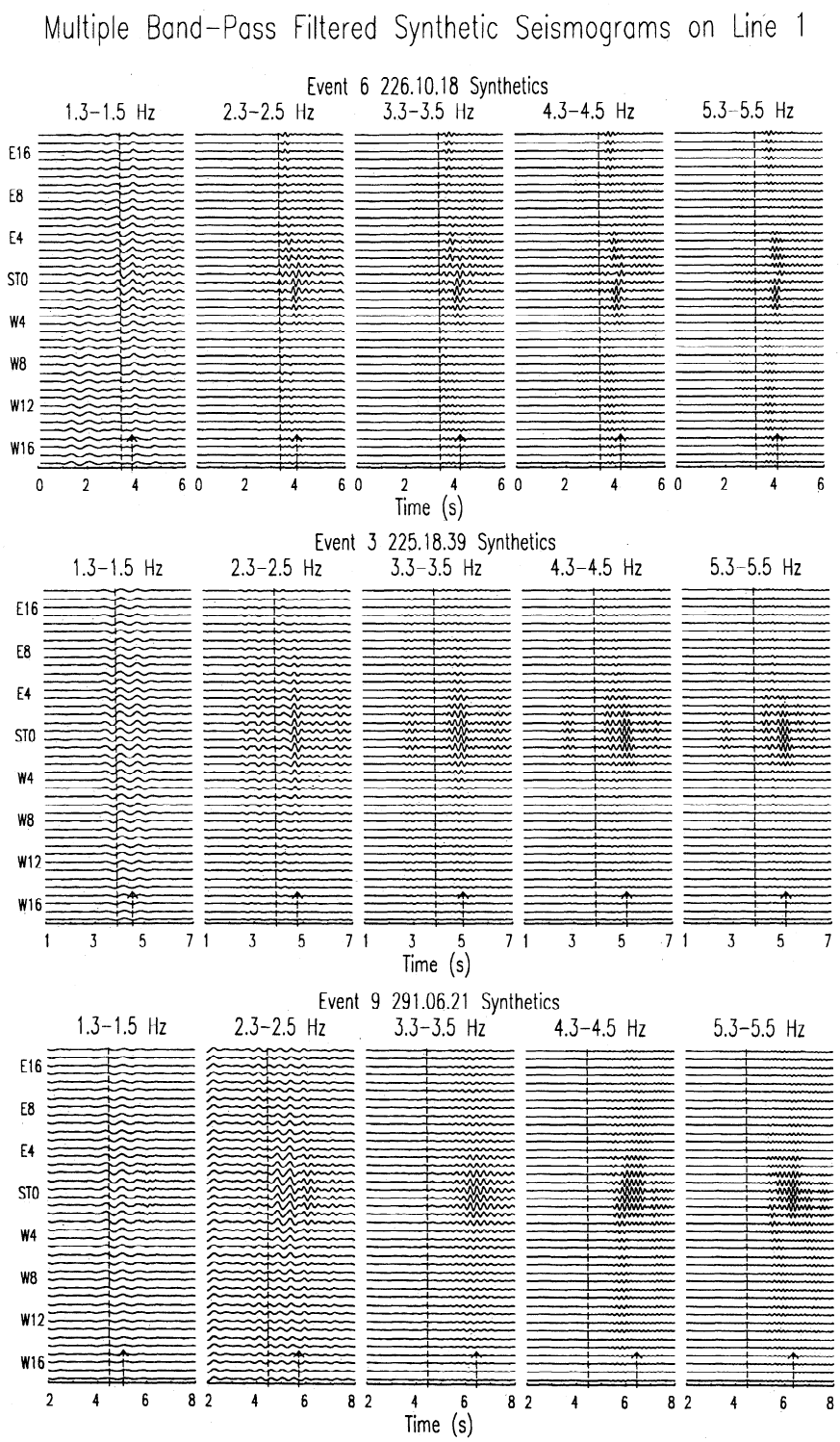

Figure 12. Multiple band-pass-filtered synthetic seismograms in five frequency bands on line 1 for events 6, 3, and 9. Seismograms are the fault zone parallel component. Bandwidth is 0.2 Hz. Synthetic band-pass seismograms show the dispersion, consistent with that of observed trapped waves as shown in Figure 6.

active fault. However, the magnitude of velocity change due to the fault healing is so small that it need not be considered in the modeling of fault zone trapped waves in this paper.

The internal structure of the Landers southern rupture revealed by fault zone trapped waves gives crucial details required for quantitative studies of earthquakes. A fuller understanding of earthquakes is useful for many reasons, such as the prediction of ground motion in future earthquakes.

Acknowledgments. This study was supported by NSF grant EAR-9804811 and the Southern California Earthquake Center under National Science Foundation Cooperative Agreement EAR-8920136 and U.S. Geological Survey Cooperative Agreements 14-08-0001 and 1434-HQ-97AG01718. We appreciate the support of IRIS-PASSCAL Instrument Center for the use of their instruments and appreciate J. Fowler, M. Alvarez, R. Sell and T. Parker for their collaboration in our experiments. Thomas Burdette of the USGS helped us to detonate explosions in the experiments. We thank D. Adams, D. Bowman, G. Ely, Z. Liu, L. Ma, A. Martin, Q. Peng, C. Wang, and J. Wedberg for their work in the field.

We are indebted to Robert Graves for his kindly offering the 3-D finite difference code used in our computation of seismograms. We also thank Robert Clayton, Steve Day, Bill Ellsworth, and Gary Fuis for their valuable suggestions. The comments of the Associate Editor Michael Kendall and two anonymous referees helped to improve this manuscript. We acknowledge the Bureau of Land Management at Barstow and many land property owners at Landers, including Edward Landau, Richard Hawley, Michael Clark, and Ann Cloutier for their permission to carry out the experiment in the public and private lands. This is SCEC contribution 478.

References

Aki, K., Characterization of barriers on an earthquake fault, *J. Geophys. Res.*, 84, 6140-6148, 1979.

Aki, K., Asperities, barriers, characteristic earthquakes, and strong motion prediction, *J. Geophys. Res.*, *89*, 5867-5872, 1984.

Aki, K., and W. H. K. Lee, Determination of three-dimensional velocity anomalies under a seismic array using first *P* arrival times from local earthquakes, 1, A homogeneous initial model, *J. Geophys. Res.*, *81*, 4381-4399, 1976.

Beck, S. L., and D. H. Christensen, Rupture process of the February 4, 1965, Rat Islands earthquake, *J. Geophys. Res.*, *96*, 2205-2221, 1991.

Ben-Zion, Y., Properties of seismic fault zone waves and their utility for imaging low-velocity structure, *J. Geophys. Res.*, *103*, 12,567-12,585, 1998.

Blanpied, M. L., D. A. Lockner, and J. D. Byerlee, An earthquake mechanism based on rapid sealing of faults, *Nature*, *359*, 574-576, 1992.

Byerlee, J., Friction, overpressure and fault-normal compression, *Geophys. Res. Lett.*, *17*, 2109-2112, 1990.

Campillo, M., and R. Archuleta, A rupture model for the 28 June, 1992 Landers, California, earthquake (abstract), *Eos Trans. AGU, 73*(43), Fall Meet. Suppl., F374, 1992.

Chester, F. M., J. P. Evans, and R. L. Biegel, Internal structure and weakening mechanisms of the San Andreas fault, *J. Geophys. Res.*, *98*, 771-786, 1993.

Cormier, V. F., and P. Spudich, Amplification of ground motion and waveform complexity in fault zones: Examples from the San Andreas and Calaveras faults, *Geophys. J. R. Astron. Soc.*, *79*, 135-152, 1984.

Cowie, P. A., and C. H. Scholz, Growth of faults by accumulation of seismic slip, *J. Geophys. Res.*, *97*, 11,085-11095, 1992.

Eberhart-Phillips, D., and A. J. Michael, Three-dimensional velocity structure, seismicity, and fault structure in the Parkfield region, central California, *J. Geophys. Res.*, *98*, 15,737-15,758, 1993.

Graves, R. W., Simulating seismic wave propagation in 3D elastic media using staggered-grid finite differences, *Bull. Seismol. Soc. Am.*, *86*, 1091-1106, 1996.

Harris, R. A., and S. M. Day, Dynamics of fault interaction: Parallel strike-slip faults, *J. Geophys. Res.*, *98*, 4461-4472, 1993.

Hough, S. E., Y. Ben-Zion, and P. Leary, Fault-zone waves observed at the southern Joshua Tree earthquake rupture zone, *Bull. Seismol. Soc. Am.*, *84*, 761-767, 1994.

Ida, Y., The maximum acceleration of seismic ground motion, *Bull. Seismol. Soc. Am.*, *63*, 959-968, 1973.

Ito, H., Structure and physical properties of the Nojima fault, paper presented at U.S.-Japan Natural Resources 10th Biennial Meeting, South. Calif. Earthquake Cent., U.S. Geol. Surv., Pasadena, Calif., 1996.

Johnson, A. M., R. W. Fleming, and K. M. Cruikshank, Shear zones formed along long, straight traces of fault zones during the 28 June 1992 Landers, California, earthquake, *Bull. Seismol. Soc. Am.*, *84*, 499-510, 1994.

Johnson, A. M., R. W. Fleming, K. M. Cruikshank, S. Y. Martosudarmo, N. A. Johnson, and K. M. Johnson, Analecta of structures formed during the 28 June 1992 Landers-Big Bear, California earthquake sequence, *U.S. Geol. Surv. Open File Rep.*, *97-94*, 59 pp., 1997.

Jongmans, D., and P. E. Malin, Microearthquake S-wave observations from 0 to 1 km in the Varian Well at Parkfield, California, *Bull. Seismol. Soc. Am.*, *85*, 1805-1820, 1995.

Kanamori, H., Mechanics of earthquakes, *Annu. Rev. Earth Planet. Sci.*, *22*, 207-237, 1994.

Leary, P. C., Y. Ben-Zion, H. Igel, and P. Mora, Modeling San Andreas fault trapped waves with a 2D analytic expression for a layered fault zone between two quarterspaces (abstract), *Eos Trans. AGU, 72*(44), Fall Meet. Suppl., F307, 1991a.

Leary, P. C., H. Igel, and Y. Ben-Zion, Observation and modeling of fault zone seismic trapped waves in aid of precise precursory microearthquake location and evaluation, paper presented at Conference on Earthquake Prediction: State-of-the Art, Strasbourg, France, Oct. 15-18, 1991b.

Lees, J. M., and P. E. Malin, Tomographic images of *P* wave velocity variation at Parkfield, California, *J. Geophys. Res.*, *95*, 21,793-21,804, 1990.

Li, Y. G., Trapped modes in a transversely isotropic fault-zone, Ph.D. thesis, pp. 168-189, Univ. of South. Calif., Los Angeles, 1988.

Li, Y. G., and P. C. Leary, Fault-zone trapped seismic waves, *Bull. Seismol. Soc. Am.*, *80*, 1245-1271, 1990.

Li, Y. G., and J. E. Vidale, Low-velocity fault-zone guided waves: Numerical investigations of trapping efficiency, *Bull. Seismol. Soc. Am.*, *86*, 371-378, 1996.

Li, Y. G., P. C. Leary, K. Aki, and P. E. Malin, Seismic trapped modes in the Oroville and San Andreas fault zones, *Science*, *249*, 763-766, 1990.

Li, Y. G., K. Aki, D. Adams, A. Hasemi, and W. H. K. Lee, Seismic guided waves trapped in the fault zone of the Landers, California, earthquake of 1992, *J. Geophys. Res.*, *99*, 11,705-11,722, 1994a.

Li, Y. G., J. E. Vidale, K. Aki, C. J. Marone, and W. H. K. Lee, Fine structure of the Landers fault zone: Segmentation and the rupture process, *Science*, *256*, 367-370, 1994b.

Li, Y. G., W. L. Ellsworth, C. H. Thurber, P. E. Malin, and K. Aki, Observations of fault-zone trapped waves excited by explosions at the San Andreas fault, central California, *Bull. Seismol. Soc. Am.*, *87*, 210-221, 1997a.

Li, Y. G., F. L. Vernon, and K. Aki, San Jacinto fault-zone guided waves: A discrimination for recently active fault strands near Anza, California, *J. Geophys. Res.*, *102*, 11,689-11,701, 1997b.

Li, Y. G., J. E. Vidale, K. Aki, F. Xu, and T. Burdette, Evidence of shallow fault zone strengthening after the 1992 *M*7.5 Landers, California, earthquake, *Science*, *279*, 217-219, 1998a.

Li, Y. G., K. Aki, J. E. Vidale, and M. G. Alvarez, A delineation of the Nojima fault ruptured in the *M*7.2 Kobe, Japan, earthquake of 1995 using fault-zone trapped waves, *J. Geophys. Res.*, *103*, 7247-7263, 1998b.

Li, Y. G., K. Aki, J. E. Vidale, and F. Xu, Shallow structure of the Landers fault zone from explosion-generated trapped waves, *J. Geophys. Res.*, *104*, 20,257-20,275, 1999.

Lindh, A., and D. M. Boore, The relation of the Parkfield foreshocks to the initiation and extent of rupture (abstract), *Earthquake Notes*, *45*, 54, 1974.

Malin, P. E., and M. Lou, A first observation of microearthquake FR waves, (abstract), *Eos Trans. AGU, 76*(46), Fall Meet. Suppl., F398, 1995.

Malin, P. E., S. N. Blakeslee, M. G. Alvarez, and A. J. Martin, Microearthquake imaging of the Parkfield asperity, *Science, 244*, 557-559, 1989.

Marone, C., Laboratory-derived friction laws and their application to seismic faulting, *Annu. Rev. Earth Planet. Sci., 26*, 643-696, 1998a.

Marone, C., The effect of loading rate on static friction and the rate of fault healing during the earthquake cycle, *Nature, 391*, 69-72, 1998b.

Marone, C., J. E. Vidale, and W. L. Ellsworth, Fault healing inferred from time dependent variations in source properties of repeating earthquakes, *Geophys. Res. Lett.*, *22*, 3095-3098, 1995.

Massonnet, D., W. Thatcher, and H. Vadon, Detection of postseismic fault-zone collapse following the Landers earthquake, *Nature, 382*, 612-616, 1996.

Michelini, A., and T. V. McEvilly, Seismological studies at Parkfield, I, Simultaneous inversion for velocity structure and hypocenters using cubic B-splines parameterization, *Bull. Seismol. Soc. Am.*, *81*, 524-552, 1991.

Mooney, W. D., and A. Ginzburg, Seismic measurements of the internal properties of fault zones, *Pure Appl. Geophys.*, *124*, 141-157, 1986.

Papageorgiou, A. S., and K. Aki, A specific barrier model for the quantitative description of inhomogeneous faulting and the prediction of strong motion, I, Description of the model, *Bull. Seismol. Soc. Am.*, *73*, 693-722, 1983.

Rice, J. R., The mechanics of earthquake rupture, in *Physics of the Earth's Interior*, edited by A. M. Dziewonski and E. Boschi, pp. 555-649, North-Holland, Amsterdam, 1980.

Rice, J. R., Fault stress states, pore pressure distributions, and the weakness of the San Andreas fault, in *Fault Mechanics and Transport Properties of Rocks*, edited by B. Evans and T.-F. Wong, pp. 475-503, Academic, San Diego, Calif., 1992.

Schlische R. W., S. S. Young, and A. Gupta, Geometry and scaling relations of a population of very small rift-related normal faults, *Geology*, *24*, 683-686, 1996.

Scholz, C. H., *The Mechanics of Earthquakes and Faulting*, Cambridge Univ. Press, New York, 1990.

Scholz, C. H., N. H. Dawers, J. Z. Yu, and M. H. Anders, Fault growth and fault sealing laws: Preliminary result, *J. Geophys. Res.*, *98*, 21,951-21,961, 1993.

Scott, J. S., T. G. Masters, and F. L. Vernon, Three-dimensional velocity structure of the San Jacinto fault zone near Anza, California, I, P-waves, *Geophys. J. Int.*, *119*, 611-626, 1994.

Sibson, R. H., Fault rocks and fault mechanisms, *J. Geol. Soc. London*, *133*, 191-213, 1977.

Sibson, R. H., Fault zone models, heat flow, and the depth distribution of earthquakes in the continental crust of the United States, *Bull. Seismol. Soc. Am.*, *151*-163, 1982.

Sieh, K. et al., Near-field investigations of the Landers earthquake sequence, April to July 1992, *Science*, *260*, 171-176, 1993.

Thurber, C. H., Earthquake locations and three-dimensional crustal

structure in the Coyote Lake area, central California, *J. Geophys. Res.*, *88*, 8226-8236, 1983.

Thurber, C. H., S. Roecker, W. Ellsworth, Y. Chen, W. Lutter, and R. Sessions, Two-dimensional seismic image of the San Andreas fault in the northern Gabilan Range, central California: Evidence for fluids in the fault zone, *Geophys. Res. Lett.*, *24*, 1591-1594, 1997.

Vermilye, J. M., and C. H. Scholz, A microstructural view of fault growth, *J. Geophys. Res. 103*, 12,223-12,238, 1998.

Vidale, J. E., W. L. Ellsworth, A. Cole, and C. Marone, Rupture variation with recurrence interval in eighteen cycles of a small earthquake, *Nature*, 368, 624-626, 1994.

Wald, D. J., and T. H. Heaton, Spatial and temporal distribution of slip for the 1992 Landers, California, earthquake, *Bull. Seismol. Soc. Am.*, *84*, 668-691, 1994.

K. Aki and Y.-G. Li, Department of Earth Sciences, University of Southern California, Los Angeles, CA 90089-0740. (ygli@terra.usc.edu; kaki@usc.edu)

J. E. Vidale and F. Xu, Department of Earth and Space Sciences, University of California, Los Angeles, CA 90095-1567. (vidale@moho.ess.ucla.edu; fxu@ess.ucla.edu)

(Received July 26, 1999; revised November 10, 1999; accepted December 17, 1999)